# Optical properties of nanostructured metal films

**P. N. Bartlett,[a] J. J. Baumberg,[b] S. Coyle[b] and M. Abdelsalem[a]**

[a] *Department of Chemistry, University of Southampton, Southampton, UK SO17 1BJ*
[b] *Department of Physics and Astronomy, University of Southampton, Southampton, UK SO17 1BJ*

***Received 14th April 2003, Accepted 19th May 2003***

Nanostructured metal films of platinum, gold and silver up to 675 nm thick we prepared by electrochemical deposition through templates of 700 nm diameter polystyrene spheres assembled as hexagonal close packed monolayer on an evaporated gold surface followed by removal of the template by dissolution in tetrahydrofuran. The reflection spectra of the films at normal incidence were recorded as a function of film thickness and the spectra correlated with the local visual appearance of the film and the surface structure from SEM. For thin films, below one quarter sphere height, the spectra show a single reflectivity dip at a wavelength just below the sphere diameter consistent with surface-plasmon grating-like behaviour. For the thicker films several reflectivity dips are observed which move towards longer wavelength with increasing film thickness. This behaviour shown to be consistent with a model in which light reflected from the top of the structure interferes with light reflected from within the spherical segment cavities in the film.

## Introduction

Spherical colloidal particles of polymers (typically polystyrene) or silica with diameters from 20 nm up to 1 μm and larger with low coefficients of variation in their diameter (often ~1.5% for polystyrene particles) are readily available either from commercial suppliers or by published syntheses.[1] As the volume fraction of particles in solution increases the particles crystallise into close packed arrays driven by maximisation of the vibrational entropy of the system.[2] These close packed arrays of uniform sub-micron particles offer an attractive and, in principle, simple means to template the three dimensional structure of a variety of materials.

Arrays of particles of this type one or two layers thick have been used as masks in lithographic processes where material was either deposited through the layer or the layer was used as an etch resist in a process sometimes referred to as "natural lithography",[3] for examples see the recent review by Burmeister *et al.*[4] The attraction of this approach is that it allows the use of sub-micron lithographic processes without the associated high cost of using X-ray or electron beam lithographic techniques.

Three dimensional close packed arrays of uniform colloidal spherical particles (artificial opals) have also attracted attention because of their potential as templates for the fabrication of photonic crystals.[5] These three dimensional colloidal particle arrays show diffractive properties (they are opalescent) and in transmission possess a stop band due to Bragg diffraction between the layers of particles in the crystal.[6–8] However for photonic crystal applications the inverse opal structure is more attractive because it has a higher proportion of void space.[5,9,10] In a three dimensional

dielectric photonic crystal it is possible for a photonic band gap to arise corresponding to a frequency range in which light will not propagate within the crystal because of multiple Bragg reflections. Interest in two and three dimensional photonic crystals is driven by the potential applications of these structures in optoelectronic devices such as integrated waveguide structures,[11] optical limiters and switches.[12] These applications require a high degree of regular packing, uniform void feature size and, in many cases, the systematic introduction of defects at particular places within the structure. There has also been interest in these inverse opal structures as materials for chemical sensors[13] or filtration,[14,15] although data on these applications is rather limited.

Inverse opals have been prepared by several groups by infiltration of the spaces between the colloidal particles in the template by precursor materials such as $Si(OH)_4$ solution,[16,17] metal alkoxides,[18–21] phenolic resin,[22] polymers[14,15,23] and semiconductor quantum dots[24] with varying degrees of success in terms of the quality and regularity of the final nanostructured material. In all these approaches the template is removed after infiltration, in the case of the silica template by dissolving in HF, in the case of the polymer template by either dissolving in a suitable organic solvent or by calcination. Complete removal of the template spheres is possible because where the spheres touch in the template structure circular ''windows'' between the spherical voids are left in the final inverse structure so that all the voids are interconnected. The diameter of these interconnecting windows depends on the method used to infiltrate the template and form the final material. After removal of the template the material is usually consolidated or converted into the final chemical form by calcination. This process often leads to significant shrinkage[16,18,19] of the structures (typically by 20 to 35%) and cracking of the sample.

Metallic inverse opal structures show different photonic properties to those fabricated from dielectric materials and are, therefore, of interest in their own right.[25–28] Structures made with features in the hundreds of nm size range should show photonic properties in the visible region of the spectrum. The first examples of metallic inverse opal structures where reported by Jiang *et al.*[29] and by Velev *et al.*[30] Jiang *et al.* used silica spheres as the template and used nanocrystal catalysed electroless deposition to infiltrate the structures with platinum, copper, nickel, gold and silver.[29,31] Velev *et al.*[30,32] used polystyrene latex templates and infiltrated the structure with colloidal gold particles. Two other approaches which have been used to prepare metallic nanostructures are the infiltration of the colloidal crystal template by an appropriate metal salt, conversion to the oxalate and then thermal decomposition to give the metal[33–35] and the direct infiltration of the template by the molten metal.[36]

The first example of electrochemical deposition through a colloidal template was reported by Braun and Wiltzius who described the electrochemical deposition of CdSe and CdS through templates assembled from 466 nm diameter polystyrene spheres assembled on a indium tin oxide electrode.[37] Subsequent work has extended this approach to the deposition of other semiconductors,[38,39] metals (notably platinum, gold, silver, cobalt, nickel tin/cobalt alloy),[40–45] metal oxides (ZnO and $PbO_2$),[46,47] and conducting polymers.[48–50] A recent review by Braun and Wiltzius concentrates on the electrochemical growth of photonic crystals.[51]

Electrochemical deposition has a number of significant advantages, particularly for the deposition of thin, supported films of macroporous materials. First, electrochemical deposition produces a high density of the deposited material within the voids of the template and leads to volume templating of the structure as opposed to templating of material around the surface of the template spheres. As a result there is no shrinkage of the material when the template is removed and no need for further processing steps or the use of elevated temperatures. In consequence the resulting metal film is a true cast of the template structure and the size of the spherical voids within the metal is directly determined by the size of template spheres used. Second, electrodeposition can be used to prepare a wide range of materials from both aqueous and non-aqueous solutions under conditions which are compatible with the template. Third, electrochemical deposition allows fine control over the thickness of the resulting macroporous film through control of the total charge passed to deposit the film. This is a unique feature of the approach. Fourth, electrochemical deposition is ideal for the production of thin supported layers for applications such as photonic mirrors since the surface of the electrochemically deposited film can be very uniform. It is also important to note that, because the template spheres are assembled onto the flat surface of the electrode and because electrochemical deposition occurs from the electrode surface out through the overlying template, the first layer of templated material, deposited out to a thickness comparable to

the diameter of the template spheres used, has a different structure from subsequent layers. Subsequent growth of the film by electrodeposition out through the template leads to a modulation of the surface topography of the film in a regular manner that will depend on the precise choice of deposition bath and deposition conditions.[45]

Despite the significant interest in photonic structures there have been very few reports of the optical properties of nanostructured metal films of this type.[36,45,52–54] In this paper we report the first results for a detailed study of the reflectance spectra of nanostructured films of platinum, gold and silver recorded at normal incidence as a function of the thickness of the nanostructured metal film.

## Experimental

### Chemicals

The templates were made of monodisperse polystyrene latex spheres (Duke Scientific Corporation) supplied as a 1 wt.% solution in water (manufacturer's certified mean diameter of 701 nm $\pm$ 6 nm, coefficient of variation in diameter 1.3%). Before use, the suspensions were homogenized by successive, gentle inversions for a couple of minutes followed by a sonication for 30 s.

All solvents and chemicals were of reagent quality and were used without further purification. The commercial cyanide free gold plating solution (Tech. Gold 25, containing 7.07 g $dm^{-3}$ gold) was obtained from Technic Inc. (Cranston, RI, USA). Hexachloroplatinic acid, $H_2PtCl_6$ (purity 99.99%), isopropanol, tetrahydrofuran (THF), cysteamine and ethanol were obtained from Aldrich. Silver was deposited from a low cyanide bath composed of 0.3027 mol $dm^{-3}$ $K_4P_2O_4$ (Aldrich), 0.1228 mol $dm^{-3}$ KCN (BDH) and 0.0185 mol $dm^{-3}$ AgCN (Aldrich). All solutions were freshly prepared using reagent-grade water (18 M$\Omega$ cm) from a Whatman RO80 system coupled to a Whatman "Still Plus" system.

### Preparation of gold substrates

Evaporated gold electrodes used as substrates were prepared by evaporating 10 nm of chromium, followed by 200 nm of gold onto 1 mm thick glass microscope slides. These gold substrates were thoroughly cleaned before use by sonication in deionized water for 30 min followed by sonication in isopropanol for 90 min. They were then rinsed with deionized water and dried under a gentle stream of argon (BOC Gases). Cysteamine was self-assembled onto the evaporated gold electrodes by immersing the freshly cleaned gold substrate in a 10 mmol $dm^{-3}$ ethanolic solution of cysteamine at room temperature for several days.

### Assembly of the colloidal templates

The deposition of the colloidal template layers was carried out in a thin layer cell (2 cm $\times$ 1.5 cm) made up of the cysteamine coated gold electrode and a clean, uncoated, microscope cover glass held 100 μm apart by a spacer cut from Parafilm (Pechiney Plastic Packaging, Inc.). The space between the two plates was filled with the aqueous 1 wt.% suspension of polystyrene latex spheres. The transparent glass plate allows the filling of cell to be monitored and a very slight argon stream was used to remove any trapped air bubbles. The filled thin layer cell was held vertically in an incubator (Model LMS series 1) in order to control the rate of evaporation from the cell. After drying the template appears opalescent with colours from green to red, depending on the angle of observation, clearly visible when illuminated from above with white light. The templates are robust and adhere well to the gold substrates. There was no evidence for re-suspension of the latex particles when placed in contact with the electroplating solutions.

### Electrochemical deposition of platinum, gold and silver

Electrochemical deposition was performed in a thermostated cell at 25 °C using a conventional three-electrode configuration controlled by an Autolab PGSTAT30. The template-coated gold

substrate was the working electrode with a large area platinum gauze counter electrode and a home-made saturated calomel reference electrode (SCE). Gold and platinum films were deposited under potentiostatic conditions at −0.95 V or 0.05 V *vs.* SCE respectively. Silver was deposited from a low cyanide plating bath using pulse plating.[55] This was chosen because other silver plating baths exhibit instability and the resulting deposits are of low quality in terms of adhesion.[56] The templated silver films were produced using galvanostatic pulse plating with the first pulse to a current density of 20 mA $cm^{-2}$ for 100 ms (this is important to ensure good adhesion) followed by a train of pulses of 5 mA $cm^{-2}$ for 50 μs separated by a rest time (*i.e.* zero current) of 1 s.

In some experiments gold, platinum and silver films were grown with a series of steps in thickness. This was achieved by withdrawing the substrate in a series of steps (each of about 500 μm) from the electrodeposition solution using a microstage. When the electrochemical deposition was complete the samples were soaked in THF for 2 h to dissolve the polystyrene template.

An environmental scanning electron microscope (Philips XL30 ESEM) was used to study the morphology and microstructure of both the polystyrene templates and the macroporous metal films.

## Optical measurements

Simultaneous visual observation and spectral analysis of small sample areas (l $\mu m^2$–100 $\mu m^2$) was achieved using an optical microscopy arrangement (BX51TRF Olympus), Fig. 1. An incoherent white light source was used to illuminate the samples and images were recorded using a CCD camera (DP2 Olympus). A fibre-coupled spectrometer (Ocean Optics, spectral range 300–1000 nm, resolution l nm) placed in the focal plane of the image was used to acquire the spectral response from the selected area (approximate diameter 50 μm at ×10 magnification). All spectra were normalised with respect to the reflection off a silver mirror, whose reflectivity over the wavelength range studied is constant. Polarisation studies and film smoothness measurements were carried out using polarisation selective optics and dark field apertures, respectively. The domain size of the macroporous regions in a template was measured through observation of diffracted wavelengths from wide-angle white light illumination and are 100–5000 μm across depending on the templating conditions.

In this study the reflection spectra at normal incidence were recorded as a function of the thickness and surface morphology of the films. To achieve this the films were grown with a series of discrete steps in thickness (see above) and reflection spectra and SEM images were recorded at known points on the sample for each step. This was achieved by using optical images of the film as a map to pin-point the locations of each measurement relative to particular defects or irregularities in the film. Replicate measurements of the reflection spectra at different regions on each step were made to confirm that the spectra were representative for each film thickness.

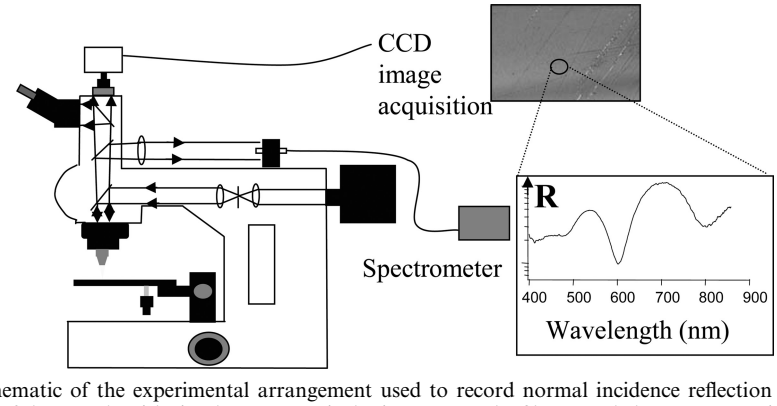


**Fig. 1** Schematic of the experimental arrangement used to record normal incidence reflection spectra from small areas of the sample with simultaneous optical microscopy. The fibre-coupled spectrometer is placed in an image plane of the sample.

## Results

### Assembly of the template

Many methods have been proposed to produce colloidal crystalline samples which are free from defects over macroscopic length scales.[57] A popular approach is to use gravity sedimentation from a dispersion of the colloid in a suitable solvent.[58–61] This yields centimetre-scale pieces of polycrystalline material but with numerous defects in the crystal lattice (stacking faults, dislocations, grain boundaries and vacancies). In addition, during gravity sedimentation it is difficult to control film thickness. Other methods for ordering colloids into arrays have been investigated. The flow of solvent through micromachined channels has been used to create dense colloidal arrays of multiple layers.[14,15,62] Recently, the strong capillary forces which develop at a meniscus between a substrate and a colloidal solution have been used to produce three dimensional arrays of controlled thickness.[63–69] If this meniscus is slowly swept across a vertically placed substrate by, for example solvent evaporation, thin planar opaline films can be deposited. A modification of this approach was used in the present work using cysteamine modified gold surfaces. The formation of close packed monolayers or multilayers of colloidal particles on the modified gold surface was achieved by careful control of the evaporation rate of the suspension. The arrangement of the spheres in the template films was investigated using high magnification scanning electron microscopy. Fig. 2a shows a top-view of a typical template assembled from 500 nm polystyrene spheres on a cysteamine treated gold surface. The spheres are close packed in a well ordered hexagonal array.

### Electrochemical deposition

Platinum, gold and silver films of controlled thickness were electrochemically deposited from aqueous solution through the pre-assembled templates. Fig. 2b shows a typical SEM image of a templated platinum film 140 nm thick grown though a template made up of a monolayer of 700 nm diameter polystyrene spheres. The micrograph shows that the spherical segment voids left in the platinum films after the removal of the polystyrene spheres have smooth and uniform mouths and

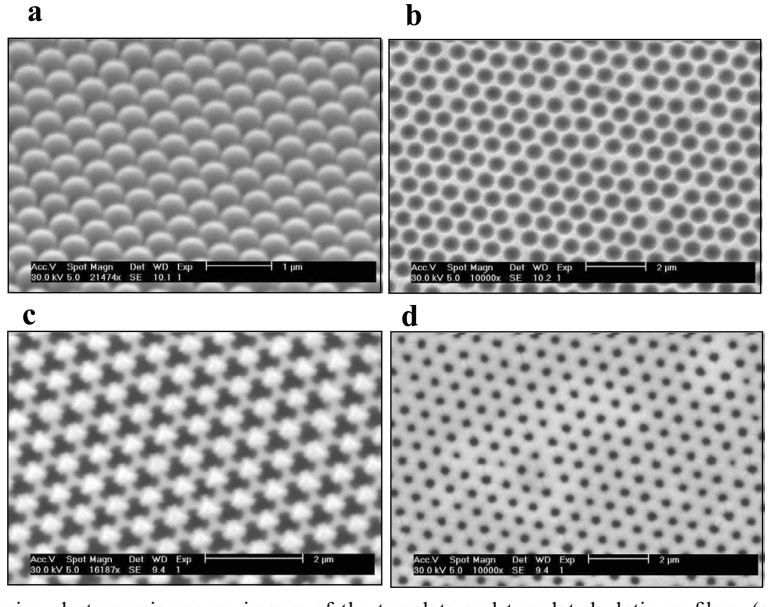


**Fig. 2** Scanning electron microscope images of the template and templated platinum films. (a) A template assembled from 500 nm diameter polystyrene spheres; (b) a 140 nm thick nanostructured platinum film deposited a 700 nm sphere diameter monolayer template; (c) 650 nm thick nanostructured platinum film deposited through a 700 nm sphere diameter multilayer template; (d) 650 nm thick nanostructured platinum film deposited through a 700 nm sphere diameter monolayer template.

are arranged in a well-ordered, close-packed, array as expected from the structure of the original template. The centre to centre distance measured for the pores in the film shown in Fig. 2b, and for similar SEM images of other films, is the same as the diameter of the polystyrene spheres used to prepare the template; thus the diameter of the spherical segment voids within the platinum film is directly determined by the diameter of the polystyrene spheres used to form the template.

Fig. 2c shows scanning electron micrograph of the top surface of a macroporous platinum film deposited through a template made up of multilayers of 700 nm diameter polystyrene spheres. In this case the platinum film was grown to be about 650 nm thick, that is approaching one template sphere in diameter. At this thickness, because of the geometry of the packing of the spheres in the template, the film starts to grow around the spheres in the second layer. As electrochemical deposition of the film proceeds out from the planar substrate, it is hindered by the polystyrene spheres in the upper layers. The presence of the template spheres in the upper layers has two effects: the spheres both block the growth of metal out from the substrate and they block diffusion of metal ions from the solution to the growing metal surface.[45] As a result the surface of the metal film is not planar and this accounts for the complex structures seen in Fig. 2c where the mouths of the pores no longer appear circular.

By controlling the number of layers of spheres in the template we are able to avoid this effect. Fig. 2d shows an SEM image for a platinum film of the same thickness but this time electrochemically deposited through a template consisting of a monolayer of 700 nm diameter polystyrene spheres. Now the mouths of the pores are nearly circular. This is because for the monolayer of polystyrene spheres there is no blocking effect from the second layer. The samples used here for reflection spectroscopy studies were all prepared using monolayer template films.

### Film thickness

Film thicknesses were calculated using the radius of the pore mouth measured in the SEM and the known radius of the template sphere. From simple trigonometry the thickness is given by

$$t = r \pm (r^2 - r_{\text{pore}}^2)^{1/2} \quad (1)$$

where $t$ is the film thickness, $r$ the radius of the template sphere and $r_{\text{pore}}$ the radius of the pore mouth. The choice sign for the $\pm$ term depends on whether the film is thicker or thinner than the radius of the template sphere.

Despite the apparent accuracy of the SEM images there is evidence from AFM cross-sections that the lips of the spherical cavities are rounded rather than sharp. This might be expected given the coupled processes of diffusion and reaction involved in the electrochemical deposition.[52] The presence of a rounded lip to the spherical segment cavity complicates the precise measurement of the pore mouth diameter in the SEM and thus the estimation of film thickness. In addition the nature of the trigonometric relation between thickness and pore mouth diameter magnifies the uncertainty in the thickness for thicknesses around one half the template sphere diameter since at this point the pore mouth diameter changes only slowly with changing thickness. These uncertainties are reflected in the estimates of film thickness given below through the values given for the estimated errors which are largest around half sphere height. Nevertheless, other methods of determining film thickness have their own drawbacks; cross-sectioning the film has the obvious disadvantage that it damages the sample, AFM measurements are problematic because as the film gets thicker, the pore mouth closes up.

### Reflection spectra of nanostructured metal films

The reflection spectra at normal incidence of the nanostructured films of platinum, gold and silver, each prepared using a monolayer template of 700 nm polystyrene spheres, were recorded as a function of film thickness. Reflection spectra for the platinum film are shown in Fig. 3 together with corresponding optical and SEM images. The optical images show the change in film colour from grey-green through red, orange and blue and then back to grey-green as the film thickness increases. The corresponding SEM images show the associated change in pore mouth diameter. The individual reflection spectra are plotted on a log-scale (off-set from one another for clarity) with the sample thickness increasing from top to bottom. Dips in reflectivity are observed which

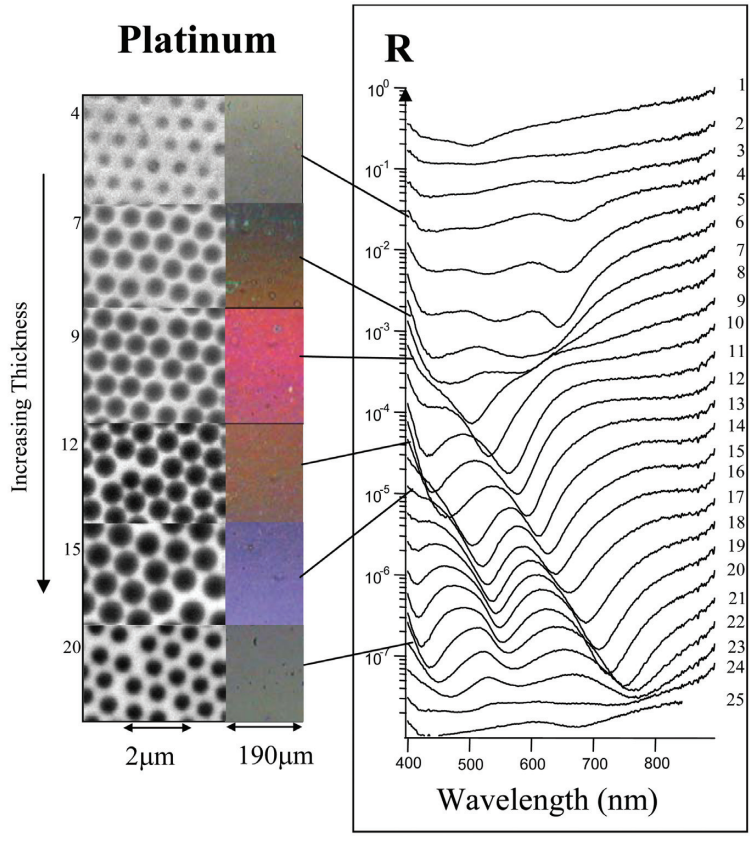


**Fig. 3** Normal incidence reflectance spectra for a stepped nanostructured platinum film grown though a 700 nm sphere diameter monolayer template together with corresponding optical and SEM images. The thickness of the sample increases down the page and the individual spectra are off-set for clarity. The errors in thickness are calculated based on an error of ±20 nm in the pore mouth radius measured from the SEM images using eqn. (1). See Table 1

shift to progressively longer wavelengths as the film thickness increases, causing the dramatic changes in the observed colour of the sample.

Looking at the data in more detail we see that below one quarter sphere height (spectra 1–7) there is a dip in reflectivity around 670 nm which grows steadily stronger as the film thickness increases and shifts towards shorter wavelengths (higher energy). Reflectivity dips at around the periodicity of the structure suggest a grating like effect. Much work has focused on the behaviour of

**Table 1** Sample thicknesses from Fig. 3

| Spectrum | Thickness/nm | Spectrum | Thickness/nm | Spectrum | Thickness/nm |
|---|---|---|---|---|---|
| 1 | 29 ± 17 | 10 | 245 ± 154 | 19 | 592 ± 42 |
| 2 | 40 ± 21 | 11 | 215 ± 105 | 20 | 624 ± 32 |
| 3 | 49 ± 24 | 12 | 242 ± 156 | 21 | 632 ± 29 |
| 4 | 71 ± 30 | 13 | 487 ± 103 | 22 | 632 ± 29 |
| 5 | 105 ± 41 | 14 | 550 ± 58 | 23 | 671 ± 17 |
| 6 | 150 ± 58 | 15 | 522 ± 73 | 24 | 661 ± 21 |
| 7 | 170 ± 68 | 16 | 550 ± 58 | 25 | 675 ± 16 |
| 8 | 175 ± 71 | 17 | 569 ± 50 | | |
| 9 | 233 ± 162 | 18 | 583 ± 46 | | |

gratings, notably by Wood who observed anomalies in the spectral intensity of different polarisations of light reflected from a grating.[70] Further research indicated that a grating, through conservation of momentum, could allow conduction electrons and light to couple together to produce a travelling wave solution along the dielectric/metal boundary, known as a surface plasmon.[71] This condition produces a coupling condition of

$$\sin(\theta) = [\varepsilon_1(\omega)/(1 + \varepsilon_1(\omega)]^{1/2} - m\lambda/d \quad (2)$$

where $\theta$ is the angle of incidence, $\varepsilon_1(\omega)$ the real part of the dielectric function of the metal, $\lambda$ the incident wavelength, $d$ the grating periodicity and $m$ is an integer. For our experiment, with $\theta$ of 0° and $d$ of 700 nm and using the appropriate values for $\varepsilon_1(\omega)$ for platinum,[72] eqn. (2) predicts a value of the wavelength of 675 nm, close to the experimentally observed values in Fig. 3. A more detailed approach to grating anomalies, involving solution of the electromagnetic field at this condition, reveals a change in the nature of the anomaly with variation in grating depth.[73] Briefly stated, the increase in depth of the groove initially strengthens the reflectivity minima and decreases its bandwidth. However, further increases in depth weaken and broaden the reflectivity dip. Although the experimental situation here is more complicated it seems reasonable to suggest that some of the features described by this theory are consistent with our data. This grating effect appears to decrease in intensity around one quarter sphere height (compare spectra 6–9) and we assume that this is because the area of the flat metal regions between the spherical pores is decreasing so that coupling to excitation of plasmons on the surface of the film decreases.

As the film becomes thicker still (spectra 8–24) dips in reflectivity appear which shift to longer wavelength as the thickness increases (for example compare spectra 11 and 18). Imaging the sample in this region at increasing magnification modifies the measured reflection spectrum; the reflectivity dips broaden and decrease in intensity, suggesting that interference or scattering effects dominate the optical response rather than absorption of light by the metal, Fig. 4. The increase in optical

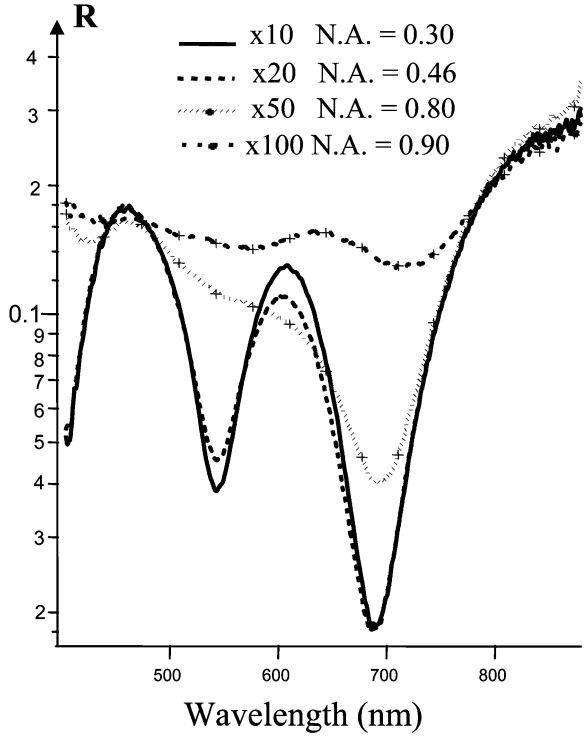


**Fig. 4** A set of normal incidence reflection spectra recorded at 4 different magnifications for a 555 nm thick nanostructured platinum film grown through a 700 nm sphere diameter monolayer template.

resolution at higher magnification separates individual ray paths, diminishing interference peaks. However this is also associated with a collection cone of greater angle (higher numerical aperture) so that scattering losses are also diminished. Consequently the data in Fig. 4 alone do not allow us to distinguish between interference and scattering effects.

In order to separate the two effects we turn to studies on samples with substantially larger spherical cavities for which the scattering due to the periodicity of the structure will be shifted into the infra-red and for which we can study the reflection properties of individual cavities. Our studies of larger metallic structures formed by electrochemical deposition of gold around 5 μm or larger diameter spheres have shown that the extreme curvature of the cavities produces unusual polarisation properties caused by a symmetric geometric reflection off the sides of each cavity.[52] Bright field images of the gold sample were taken through collinear polarisers, Fig. 5(a), and through crossed polarisers, Fig. 5(b), with the incident polarisation set to be vertical with respect to the images. Collinear polarisers only image cavity reflections which preserve the polarisation state, such as that from the single reflection off the bottom of the cavity. Light experiencing a multiple reflection off the sides of the cavity acquires a more complicated polarisation state depending on where on the sphere segment the light hits with respect to its polarisation. In Fig. 5 the polarisation state is preserved for light hitting the top, bottom, left and right sides of the micro-reflector. At other positions on the sides of the reflector (*i.e.* along the diagonal orientation) the polarisation is rotated. The origin of the polarisation rotation is geometric; at each interface the light picks up a twist in linear polarisation due to the out-of-plane reflection geometry. Polarisation studies of our sub-micron structures have also revealed the presence of these novel two reflection polarisation rotations.

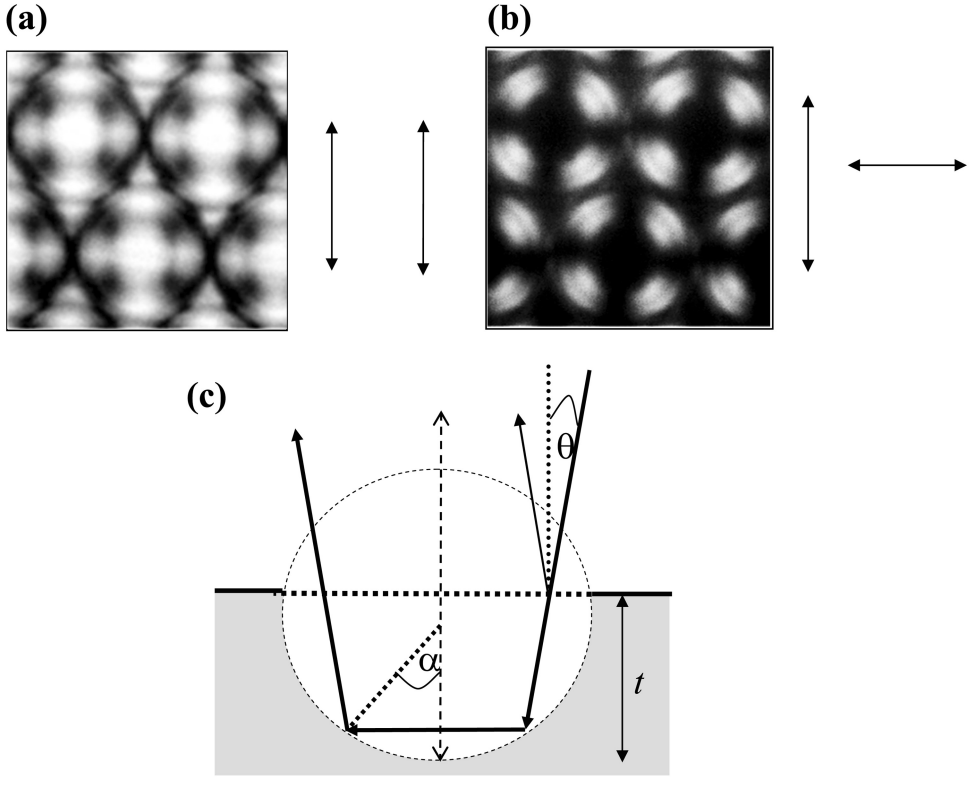


**Fig. 5** Bright field reflection images of 5 μm cavities viewed at ×200 magnification through (a) collinear and (b) crossed polarisers. (c) Ray paths of reflections of an incident plane wave off the cavity surface.

Assuming that interference effects dominate, the reflection spectra of the platinum surfaces can be modelled as an interference effect between reflections off the top of the structure and off the curved surfaces within the pores. The only reflections whose path lengths are included in the calculation are those that collimate the incident beam on reflection, Fig. 5 (c), as these paths are collected by the measurement optics with the greatest efficiency. Simulations using this model are based on calculating the effects of interference between reflections from the top surface of the film between the cavities and one and two bounce reflections from the cavities. The combined electric fields for the one and two bounce reflection models are given by

$$R_{\text{single}} = R_{\text{m}}(\theta,\lambda)\exp(\text{i}\phi(\theta,\lambda) + R_{\text{m}}(\theta,\lambda)\exp(\text{i}\pi L/\lambda + \text{i}\pi + \text{i}\phi_{\text{m}}(\theta,\lambda)) \quad (3)$$

$$R_{\text{double}} = R_{\text{m}}(\theta,\lambda)\exp(\text{i}\phi(\theta,\lambda) + R_{\text{m}}(\theta,\lambda)^2\exp(2\text{i}\pi L/\lambda + \text{i}\pi + 2\text{i}\phi_{\text{m}}(\theta,\lambda)) \quad (4)$$

where $R_{\text{single}}$ and $R_{\text{double}}$ are the reflected fields produced by either a single and double reflection within the cavity and from top surface of the film, $R_{\text{m}}(\theta,\lambda)$ is the metal reflectivity, $\theta$ is the angle of incidence, $\phi(\theta,\lambda)$ is the phase change on reflection from the metallic surface, and $L$ is the extra path length travelled in the cavity. An extra factor of $\pi$ is included in the calculation to take account of the Gouy shift associated with a beam passing through a focal point.[55] Reflections off the base of the cavity focus and diverge, whereas a double reflection off the cavity focuses and re-collimates incident light. Interference effects of single reflections are therefore likely to have a weaker presence than double reflections.

Eqns. (3) and (4) were used to calculated the predicted reflection spectra at normal incidence for platinum films of varying thickness containing 700 nm diameter spherical segment cavities using the known wavelength dependence for the reflectivity of platinum,[53] (Fig. 6) together with literature values for the reflection induced phase change, $\phi(\theta,\lambda)$.[74] The results are shown in Fig. 7. From the figure we can see that the double bounce model shows a better match to the experimental data.

The reflection spectra of the corresponding nanostructured gold film shows very similar features to those discussed above for platinum, Fig. 8. Again for thin films (spectra 1–8) there is a dip in reflectivity around 670 nm which grows steadily stronger as the film thickness increases and shifts towards shorter wavelengths. whereas for the thicker films (spectra 11–22) dips in reflectivity appear which shift to longer wavelength as the thickness increases. The differences in detail between the platinum and gold samples, and the reason why the gold exhibits the rich red colour for films around 500 nm thick, can be attributed to the differences in the reflectivity profiles (see Fig. 6) and reflection induced phase changes for the two metals. Thus our model of a surface-plasmon grating effect which is dominant for the thin films and a double bounce reflection interference effect for the thicker films can also explain the reflection spectra of the nanostructured gold film.

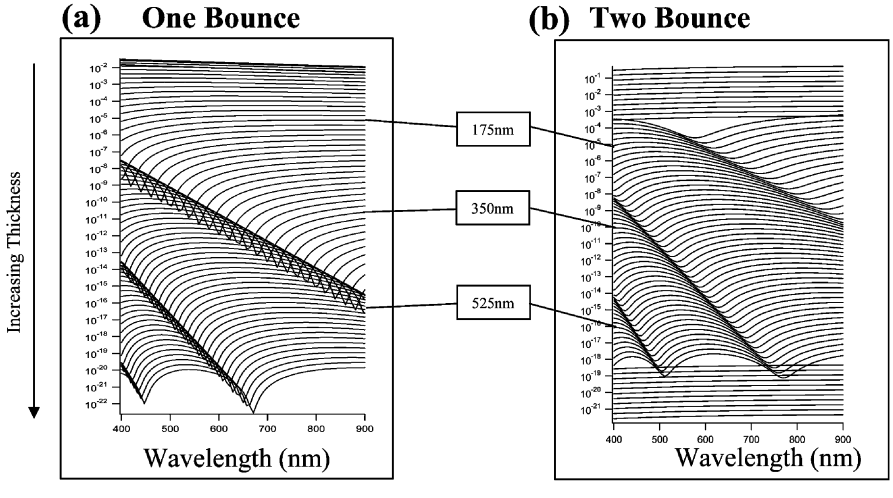


**Fig. 6** Calculated reflectivity for bulk samples of platinum, gold and silver based on literature data.[72]

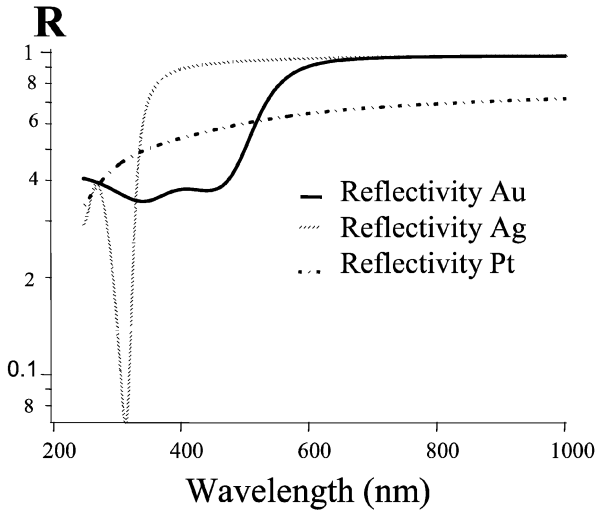


**Fig. 7** Calculated reflection spectra for platinum films grown through a 700 nm sphere diameter template using eqns. (2) and (3) for (a) the single and (b) the double bounce model. The spectra are calculated for 10 nm increments in film thickness and are offset for clarity.

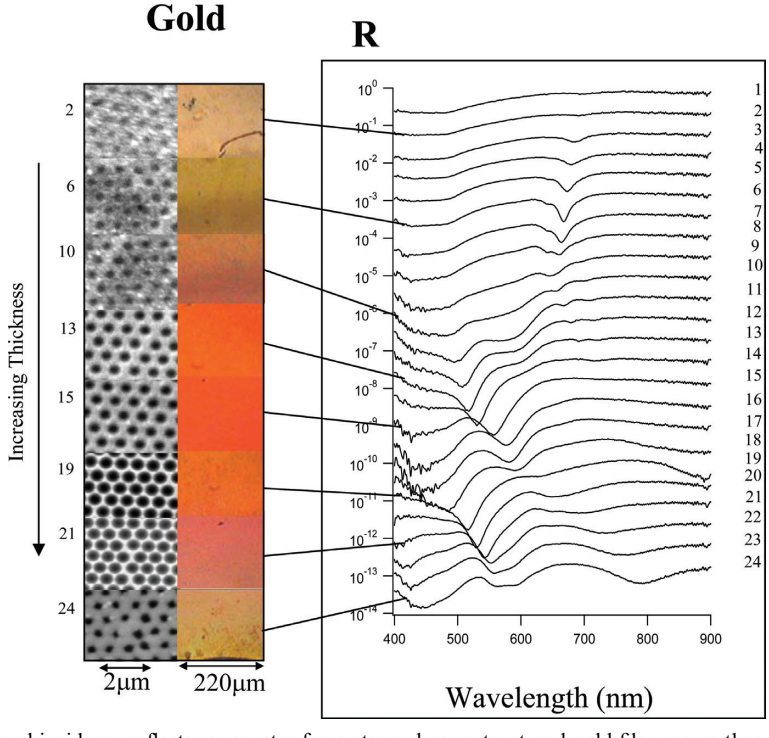


**Fig. 8** Normal incidence reflectance spectra for a stepped nanostructured gold film grown through a 700 nm sphere diameter monolayer template together with corresponding optical and SEM images. The thickness of the sample increases down the page and the individual spectra are off-set for clarity. The errors in thickness are calculated based on an error of ±20 nm in the pore mouth radius measured from the SEM images using eqn. (1). See Table 2

**Table 2** Sample thicknesses from Fig. 8

| Spectrum | Thickness/nm | Spectrum | Thickness/nm | Spectrum | Thickness/nm |
|---|---|---|---|---|---|
| 1 | $42 \pm 22$ | 9 | $100 \pm 39$ | 17 | $550 \pm 59$ |
| 2 | $45 \pm 23$ | 10 | $99 \pm 39$ | 18 | $550 \pm 59$ |
| 3 | $63 \pm 28$ | 11 | $127 \pm 49$ | 19 | $550 \pm 59$ |
| 4 | $72 \pm 31$ | 12 | $127 \pm 49$ | 20 | $657 \pm 51$ |
| 5 | $82 \pm 34$ | 13 | $220 \pm 113$ | 21 | $573 \pm 49$ |
| 6 | $84 \pm 34$ | 14 | $480 \pm 113$ | 22 | $583 \pm 45$ |
| 7 | $91 \pm 36$ | 15 | $503 \pm 87$ | 23 | $624 \pm 32$ |
| 8 | $91 \pm 36$ | 16 | $522 \pm 73$ | 24 | $626 \pm 31$ |

Finally Fig. 9 shows the corresponding data for a silver film grown through a monolayer template assembled from 700 nm diameter polystyrene spheres. In this case the reflection spectra are much less rich in structure and show only a single band around 650 nm. In contrast to the platinum and gold samples the surface of the silver sample is much rougher as shown both by the SEM images and by the optical images (compare Fig. 9 with Figs. 3 and 8). Comparison of dark field images of the silver and platinum samples at high magnification reveals distinct differences between the two sets of cavities. For the platinum the cavities are dark indicating a low level of scattering and therefore a smooth surface, for the silver sample the cavities are bright, indicating random scattering off a rough surface. This emphasises the importance of choosing the correct plating conditions in order to prepare the samples. The reflection spectra of the rough silver films is consistent with the model presented above to explain the spectra of the platinum and gold films; when the film is rough the interference effects between light reflected from within the cavities and from the top of the film are not observed and only the grating effect is seen.

### Comparison to previous work

The results presented here are the first systematic studies of the reflection spectra of metallic films with an inverse opal structure. Velev *et al.* reported that their templated gold samples showed brightly coloured reflection but did not carry out any spectral studies.[30] Kulinowski *et al.* showed

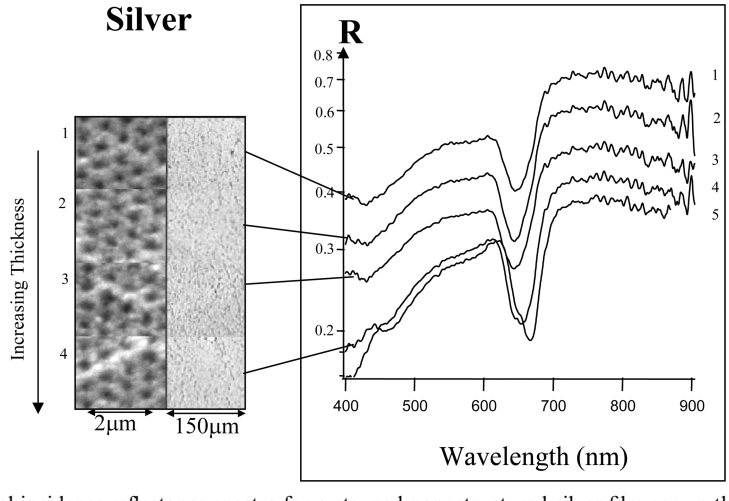


**Fig. 9** Normal incidence reflectance spectra for a stepped nanostructured silver film grown though a 700 nm sphere diameter monolayer template together with corresponding optical and SEM images. The thickness of the sample increases down the page and the individual spectra are off-set for clarity. The errors in thickness are calculated based on an error of $\pm 20$ nm in the pore mouth radius measured from the SEM images using eqn. (1). See Table 3

**Table 3** Sample thicknesses from Fig. 9

| Spectrum | Thickness/nm | Spectrum | Thickness/nm |
|---|---|---|---|
| 1 | $27 \pm 17$ | 4 | $105 \pm 41$ |
| 2 | $50 \pm 24$ | 5 | $178 \pm 73$ |
| 3 | $70 \pm 30$ | | |

reflectance data for two platinum films with different pores sizes recorded at 44° incidence with the light collected at 65°.[31] Eradat *et al.* published reflection spectra for an antimony inverse opal structure.[52] However in all these studies there was no attempt to correlate the observed spectra and the surface topography of the sample.

In earlier studies in Southampton we have studied the reflection spectra of templated gold structures.[50,51] In those experiments we observed strong dips in reflectivity that were insensitive to changes in the film thickness above one half template sphere height. Similar strong dips in the reflection spectra of the gold film are not seen in the present study. Several comments on this apparent discrepancy need to be made. First, the two sets of data are obtained at completely different angles of incidence; in the present case all measurements were made at normal incidence whereas the earlier studies were carried out using a different optical arrangement at an angle of incidence of 45°. If we consider the double bounce model, we find that increasing the angle of incidence increases the range of thicknesses for which the ray paths are blocked by the aperture of the spherical segment pore. This is shown in Fig. 10 where we plot the values of angle of incidence and dimensionless film thickness (film thickness divided by template sphere diameter) for which all geometrical reflections can take place (white), only single reflections can take place (dark

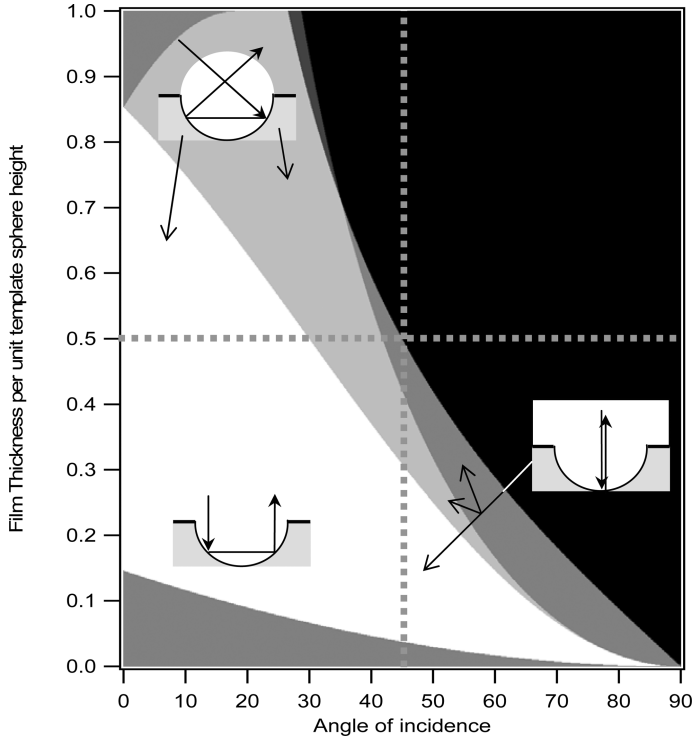


**Fig. 10** Plot of the different ranges of values of normalised film thickness and angle of incidence for which different geometrical reflection modes are possible. White: all reflections possible; dark grey: only single bounce possible; light grey: single and reverse double bounce possible; black: no reflections possible. The different reflection modes are shown by the inset cartoons.

grey) or single and reverse double reflections can take place (light grey): a reverse double reflection is one in which the ''far'' side of the cavity reflects an incoming ray to the ''near'' side of the cavity as shown in the insets in the figure. The black areas in Fig. 10 indicate ranges of film thickness and incident angle for which the ray optic model cannot be used and interference between reflections from the top and inner cavity surfaces is not possible. The strong reflectance dips reported in our earlier work[53,54] correspond to measurements in the top left hand quadrant of Fig. 10, just to the left of the vertical grey dotted line, in the black region. At higher angles of incidence reflections from the cavity become more complicated and cannot be explained using a simple geometric model. We believe a full electromagnetic solution incorporating the behaviour of confined plasmons, grating anomalies, and the effect of multiple bounce interference are required to fully explain reflection spectra at any angle. This work is currently in progress.

A second significant difference between the samples used here and those in our previous work is that in the present work we used samples produced using a well packed monolayer template rather than a multilayer template. The present films therefore have a different surface topography (see Fig. 2c and discussion above) and are more regularly packed. This increase in the quality of the films is especially marked for the platinum samples, where in an earlier preliminary study we did not observe the optical effects found here at normal incidence.[45] This emphasises the condition for smooth inner surfaces in order to observe the reflective interference phenomena observed here.

## Conclusions

In this paper we have reported the first systematic study as a function of film thickness of the normal incidence reflection spectra for nanostructured platinum and gold films templated by regular hexagonally close packed monolayers of 700 nm spherical particles. Using a microscope and fibre-coupled optic spectrometer we are able to acquire local optical images and spectra from small well defined areas of the sample and to directly correlate these with SEM images of the same regions.

Several features emerge from this study. First the use of monolayer templates, as opposed to multilayer templates, leads to a different surface topography for films over one half template sphere in thickness. Second the roughness of the electrodeposited films has a significant effect on the reflection spectra. Smooth, high quality films are essential in order to observed all of the detail in the spectra. For thin films, below one quarter sphere height we observe a surface-plasmon grating with the position of the reflectance dip consistent with the predictions of a simple grating scattering model. As the films grow thicker this grating effect disappears, possibly because the diminution in the area of the surface between the pores makes it more difficult to couple into plasmon on the surface of the film.

For film thicknesses above about one half template sphere height the reflectance spectra are dominated by a series of reflectance dips which shift to longer wavelength with increasing film thickness. These features are consistent with the predictions of a model in which there is interference between light reflected from the surface of the film and light doubly reflected within the spherical segment cavities within the film. The difference between the normal incidence reflection spectra for the platinum and gold films can be explained in terms of the differences in the reflection spectra and change in polarisation on reflection for the two metals.

From our experiments it is clear that in order to describe the reflection spectra at all angles and for all film thicknesses up to one sphere height for these samples it is be necessary to develop a full electromagnetic model which takes account of the grating effects the reflection interference effects and the effects of confined plasmons. This remains a significant theoretical challenge. Nevertheless our experiments have shown that this is a rich field for further study and that it is possible to manipulate the reflection spectra of nanostructured metal films through control of the metallic nanostructure. This suggests that films of this type may find application as components in optoelectronic and biophotonic devices.

## Acknowledgements

This work was supported by EPSRC Grant GR/R54194/01.

## References


1 M. Bardosova and R. H. Tredgold, *J. Mater. Chem.*, 2002, **12**, 2835.
2 D. Frenkel, *Phys. World*, 1993, **6**, 24.
3 H. W. Deckman and J. H. Dunsmuir, *Appl. Phys. Lett.*, 1982, **41**, 377.
4 F. Burmeister, C. Schäfle, B. Keilhofer, C. Bechinger, J. Boneberg and P. Leiderer, *Adv. Mater.*, 1998, **10**, 495.
5 J. D. Joannopoulos, R. D. Meade, and J. N. Winn, *Photonic Crystals*, Princeton University Press, Princeton, NJ, 1995.
6 Y. A. Vlasov, M. A. Kaliteevski and V. V. Nikolaev, *Phys. Rev. B*, 1999, **60**, 1555.
7 H. Míguez, C. López, F. Meseguer, A. Blanco, L. Vázquez, R. Mayoral, M. Orcaña, V. Fornés and A. Mifsud, *Appl. Phys. Lett.*, 1997, **71**, 1148.
8 B. Gates and Y. Xia, *Adv. Mater.*, 2000, **12**, 1329.
9 K. Busch and S. John, *Phys. Rev. E.*, 1998, **58**, 3896.
10 R. Biswas, M. Sigalas, G. Subramania and K.-M. Ho, *Phys. Rev. B*, 1998, **57**, 3701.
11 S.-Y. Lin, E. Chow, V. Hietala, P. R. Villeneuve and J. D. Joannopoulos, *Science*, 1998, **282**, 274.
12 M. Scalora, J. P. Dowling, C. M. Bowden and M. J. Bloemer, *Phys. Rev. Lett.*, 1994, **73**, 1368.
13 R. W. J. Scott, S. M. Yang, G. Chabanis, N. Coombs, D. E. Williams and G. A. Ozin, *Adv. Mater.*, 2001, **13**, 1468.
14 S. H. Park and Y. Xia, *Chem. Mater.*, 1998, **10**, 1745.
15 S. H. Park and Y. Xia, *Adv. Mater.*, 1998, **10**, 1045.
16 O. D. Velev, T. A. Jede, R. F. Lobo and A. M. Lenhoff, *Nature*, 1997, **389**, 447.
17 O. D. Velev, T. A. Jede, R. F. Lobo and A. M. Lenhoff, *Chem. Mater.*, 1998, **10**, 3597.
18 J. E. G. J. Wijnhoven and W. L. Vos, *Science*, 1998, **281**, 802.
19 B. T. Holland, C. F. Blanford and A. Stein, *Science*, 1998, **281**, 538.
20 B. T. Holland, C. F. Blanford, T. Do and A. Stein, *Chem. Mater.*, 1999, **11**, 795.
21 H. Yan, C. F. Blandford, B. T. Holland, W. H. Smyrl and A. Stein, *Chem. Mater.*, 2000, **12**, 1134.
22 A. A. Zakhidov, R. H. Baughman, Z. Iqbal, C. Cui, I. Khayrullin, S. O. Dantas, J. Marti and V. G. Ralchenko, *Science*, 1998, **282**, 897.
23 P. Jiang, B. J. Hwang, D. M. Mittleman, J. F. Bertone and V. L. Colvin, *J. Am. Chem. Soc.*, 1999, **121**, 11 630.
24 Y. A. Vlasov, N. Yao and D. J. Norris, *Adv. Mater.*, 1999, **11**, 165.
25 A. R. McGurn and A. A. Maradudin, *Phys. Rev. B*, 1993, **48**, 17 576.
26 D. F. Sievenpiper, M. E. Sickmiller and E. Yablonovitch, *Phys. Rev. Lett.*, 1996, **76**, 2480.
27 A. Moroz, *Phys. Rev. Lett.*, 1999, **83**, 5274.
28 A. Moroz, *Europhys. Lett.*, 2000, **50**, 466.
29 P. Jiang, J. Cizeron, J. F. Bertone and V. L. Colvin, *J. Am. Chem. Soc.*, 1999, **121**, 7957.
30 O. D. Velev, P. M. Tessier, A. M. Lenhoff and E. W. Kaler, *Nature*, 1999, **401**, 548.
31 K. M. Kulinowski, P. Jiang, H. Vaswani and V. L. Colvin, *Adv. Mater.*, 2000, **12**, 833.
32 P. M. Tessier, O. D. Velev, A. T. Kalambur, J. F. Rabolt, A. M. Lenhoff and E. W. Kaler, *J. Am. Chem. Soc.*, 2000, **112**, 9554.
33 H. Yan, C. F. Blanford, W. H. Smyrl and A. Stein, *J. Chem. Soc., Chem. Comm.*, 2000, 1477.
34 H. Yan, C. F. Blanford, J. C. Lytle, C. B. Carter, W. H. Smyrl and A. Stein, *Chem. Mater.*, 2001, **13**, 4314.
35 H. Yan, C. F. Blanford, B. T. Holland, M. Parent and W. H. Smyrl, *Adv. Mater.*, 1999, **11**, 1003.
36 A. A. Zakhidov, R. H. Baughman, I. I. Khayrullin, I. A. Udod, M. Kozlov, N. Eradat, V. Z. Vardeny, M. Sigalas and R. Biswas, *Synth. Met.*, 2001, **116**, 419.
37 P. V. Braun and P. Wiltzius, *Nature*, 1999, **402**, 603.
38 Y.-C. Lee, T.-J. Kuo, C.-J. Hsu, Y.-W. Su and C.-C. Chen, *Langmuir*, 2002, **18**, 9942.
39 L. K. van Vugt, A. F. van Driel, R. W. Tjerkstra, L. Bechgar, W. L. Vos, D. Vanmaekelbergh and J. J. Kelly, *J. Chem. Soc., Chem. Commun.*, 2002, 2054.
40 C. Lellig, W. Härtl, J. Wagner and R. Hempelmann, *Angew. Chem., Int. Ed. Engl.*, 2002, **41**, 102.
41 T. Sumida, Y. Wada, T. Kitamura and S. Yanagida, *Langmuir*, 2002, **18**, 3886.
42 Q. Luo, Z. Liu, L. Li, S. Xie, J. Kong and D. Zhao, *Adv. Mater.*, 2001, **13**, 286.
43 J. E. G. J. Wijnhoven, S. J. M. Zevenhuizen, M. A. Hendriks, D. Vanmaekelbergh, J. J. Kelly and W. L. Vos, *Adv. Mater.*, 2000, **12**, 888.
44 P. N. Bartlett, P. R. Birkin and M. A. Ghanem, *J. Chem. Soc., Chem. Comm.*, 2000, 1671.
45 P. N. Bartlett, J. J. Baumberg, P. R. Birkin, M. A. Ghanem and M. C. Netti, *Chem. Mater.*, 2002, **14**, 2199.
46 T. Sumida, Y. Wada, T. Kitamura and S. Yanagida, *Chem. Lett.*, 2001, 38.
47 P. N. Bartlett, T. Dunford and M. A. Ghanem, *J. Mater. Chem.*, 2002, **12**, 3130.
48 T. Cassagneau and F. Caruso, *Adv. Mater.*, 2002, **14**, 34.
49 P. N. Bartlett, P. R. Birkin, M. A. Ghanem and C. S. Toh, *J. Mater. Chem.*, 2001, **11**, 849.
50 T. Sumida, Y. Wada, T. Kitamura and S. Yanagida, *Chem. Commun.*, 2000, 1613.
51 P. V. Braun and P. Wiltzius, *Curr. Opin. Colloid Interface Sci.*, 2002, **7**, 116.
52 N. Eradat, J. D. Huang, Z. V. Vardeny, A. A. Zakhidov, I. Khayrullin, I. Udod and R. H. Baughman, *Synth. Met.*, 2001, **116**, 501.

53 S. Coyle, M. C. Netti, J. J. Baumberg, M. A. Ghanem, P. R. Birkin, P. N. Bartlett and D. M. Whittaker, *Phys. Rev. Lett.*, 2001, **8717**, 6801.
54 M. C. Netti, S. Coyle, J. J. Baumberg, M. A. Ghanem, P. R. Birkin, P. N. Bartlett and D. M. Whittaker, *Adv. Mater.*, 2001, **13**, 1368.
55 H. Sánchez, E. Chainet, B. Nguyen, P. Ozil and M. Meas, *J. Electrochem. Soc.*, 1996, **143**, 2799.
56 M. Schlesinger and M. Paunovic, *Modern Electroplating*, Wiley, Chichester, 2000.
57 Y. A. Vlasov, V. N. Astratov, A. V. Baryshev, A. A. Kaplyanski, O. Z. Karimov and M. F. Limonov, *Phys. Rev. E*, 2000, **61**, 5784.
58 K. E. Davis, W. B. Russel and W. J. Glantschnig, *J. Chem. Soc., Faraday Trans.*, 1991, **87**, 411.
59 R. Mayoral, J. Requena, J. S. Moya, C. Lopez, A. Cintas, H. Miguez, F. Meseguer, L. Vazquez, M. Holgado and A. Blanco, *Adv. Mater.*, 1997, **9**, 257.
60 H. Miguez, F. Meseguer, C. Lopez, A. Blanco, J. S. Moya, J. Requena, A. Mifsud and V. Fornes, *Adv. Mater.*, 1998, **10**.
61 P. Pieranski, *Contemp. Phys.*, 1983, **24**, 25.
62 S. H. Park and Y. Xia, *Langmuir*, 1999, **15**, 266.
63 P. Jiang, J. F. Bertone, K. S. Hwang and V. L. Colvin, *Chem. Mater.*, 1999, **11**, 2132.
64 A. S. Dimitrov, T. Miwa and K. Nagayama, *Langmuir*, 1999, **15**, 5257.
65 A. S. Dimitrov and K. Nagayama, *Chem. Phys. Lett.*, 1995, **243**, 462.
66 K. Nagayama, *Colloids Surf. A*, 1996, **109**, 363.
67 A. S. Dimitrov and K. Nagayama, *Langmuir*, 1996, **12**, 1303.
68 N. D. Denkov, O. D. Velev, P. A. Kralchevsky, I. B. Ivanov, H. Yoshimura and K. Nagayama, *Nature*, 1993, **361**, 26.
69 Y. A. Vlasov, X.-Z. Bo, J. C. Sturm and D. J. Norris, *Nature*, 2001, **414**, 289.
70 R. W. Wood, *Phys. Rev.*, 1935, **48**, 928.
71 M. C. Hutley, *Diffraction Grating*, Academic Press, New York, 1982.
72 A. D. Rakic, A. B. Djurisic, J. M. Elzar and M. L. Majewski, *Appl. Optics*, 1998, **37**, 5271.
73 R. Petit, *Electromagnetic Theory of Gratings*, Springer-Verlag, Berlin, 1980.
74 M. Born and E. Wolf, *Principles of Optics*, Pergamon Press, Oxford, 1970.